Spherical neutron star collapse toward a black hole in a tensor-scalar theory of gravity

Jérôme Novak
Département d'Astrophysique Relativiste et de Cosmologie, UPR 176 du CNRS, Observatoire de Paris, F-92195 Meudon Cedex, France
(Received 15 May 1997; published 12 March 1998)

Complete tensor-scalar and hydrodynamic equations are presented and integrated, for a self-gravitating perfect fluid. The initial conditions describe an unstable-equilibrium neutron star configuration, with a polytropic equation of state. They are necessary in order to follow the gravitational collapse (including full hydrodynamics) of this star toward a black hole and to study the resulting scalar gravitational wave. The amplitude of this wave, as well as the radiated energy, dramatically increases above some critical value of the parameter of the coupling function, due to the spontaneous scalarization, an effect not present in Brans-Dicke theory. In most cases, the pressure of the collapsing fluid does not have a significant impact on the resulting signal. These kinds of sources are not likely to be observed by future laser interferometric detectors (such as VIRGO or LIGO) of gravitational waves, if they are located at more than a few 100 kpc. However, spontaneous scalarization could be constrained if such a gravitational collapse is detected by its quadrupolar gravitational signal, since this latter is quite lower than the monopolar one. [S0556-2821(98)03608-X]

PACS number(s): 04.30.Db, 02.70.Hm, 04.25.Dm, 04.50.+h

I. INTRODUCTION

In order to test general relativity, one has to compare it to other, alternate theories of gravitation. *Tensor-scalar* theories, in which gravity is described by a spin-2 field combined with one or several spin-0 fields, are not only alternate theories, but ''generalize general relativity'' (see [1]), meaning that general relativity is obtained in them by setting all scalar fields to zero. Several such theories have been developed, from Fierz [2], Jordan [3], Brans and Dicke [4] to Bergman [5], Nordtvedt [6], Wagoner [7] and, more recently, Damour and Esposito-Farèse [1]. In all these theories, the spin-0 and spin-2 fields (φ and $g_{\mu\nu}$) are coupled to matter via an effective metric tensor $\tilde{g}_{\mu\nu}=a^2(\varphi)g_{\mu\nu}$. The Jordan-Fierz-Brans-Dicke theory has only one free parameter ω, whereas for Bergman, Nordtvedt, and Wagoner the parameter is a function $\omega(\varphi)$. Damour and Esposito-Farèse considered an arbitrary number of scalar fields, coupled one to the other. All these theories are motivated by, mainly, two theoretical reasons: (1) they represent the low-energy limit of superstring theories ([8] and [9]); (2) they give rise to new ''extended'' inflationary models [10].

Since in Brans-Dicke theory $\ln[a(\varphi)]$ is a linear function of φ, solar system experiments (weak field) are sufficient to constrain the theory, even in strong fields. Nevertheless, a more general theory, in which $\ln[a(\varphi)]$ is a parabolic function (depending on two parameters), shows nonperturbative effects in strong field [11], described as ''spontaneous scalarization'' in [12]. Thus, when describing neutron stars, general relativity and tensor-scalar theory can give significant differences for their masses, radii, and gravitational fields, whereas the difference can still be negligible in our solar system data. As a consequence, weak-field experiments *cannot* give much information on strong-field regime, and one needs to test this strong-field regime by other means. First, by looking for the orbital decay of binary-pulsar systems; this has been done by Damour and Esposito-Farèse ([1] and [12]), who constrained the parameter space of the coupling function. Second, by looking for monopolar gravitational radiation from collapsing compact sources which could be detected by the laser interferometric gravitational wave observatories [such as VIRGO [13] and Laser Interferometric Gravitational Wave Observatory (LIGO) [14]].

This latter method requires that the signal be known and that the observed (or unobserved) amplitude be related to the coupling function parameters. Such computations have already been performed by various groups, but they all considered only an Oppenheimer-Snyder collapse (i.e., ''dust'' matter, with no pressure), either in Brans-Dicke theory ([15] and [16]) or by doing some Taylor expansion of the coupling function [17]. In the latter, the parameter space of the coupling function was restricted to the part where nonperturbative strong-fields effects do not happen. The aim of this paper is to present the results of computations of a spherically symmetric collapse, of a neutron star toward a black hole,[1] with one scalar field and an arbitrary coupling function. All the hydrodynamics and field equations are treated with no approximation in order to get the monopolar gravitational wave form and amplitude. Moreover, including the equation of state allows us to start the collapse with quite a realistic neutron star configuration and thus, spurious waves signals are avoided (see Sec. III C).

The paper in organized as follows. Section II describes the evolution equations for the star. Section III gives the numerical results: initial-value models (Sec. III A), collapse and resulting wave signal (Sec. III B), comparison with previous works (Sec. III C), and exploration of the parameter space (Sec. III D). Finally Sec. IV gives some concluding remarks.

[1]Numerically, the black hole is never obtained, but the monopolar gravitational waves, far from the source, behave as if the black hole had formed (see Sec. III B).

II. FIELD AND HYDRODYNAMIC EQUATIONS

A. General equations

As has been stated before, the most general theory containing a spin-2 field and one (massless) spin-0 field contains one arbitrary coupling function $a(\varphi)$. The action is given by

$$S=(16\pi G_*)^{-1}\int d^4x\ \sqrt{-g_*}(R_*-2g_*^{\mu\nu}\partial_\mu\varphi\partial_\nu\varphi) + S_m[\Psi_m,a^2(\varphi)g^*_{\mu\nu}], \tag{2.1}$$

where all quantities with asterisks are related to the ''Einstein metric'' $g^*_{\mu\nu}$, G_* is the bare gravitational coupling constant, $R_*=g_*^{\mu\nu}R^*_{\mu\nu}$ the curvature scalar for this metric, and $g_*=\det(g^\mu_{*\nu})$. The term S_m denotes the action of the matter, represented by the fields Ψ_m, which is coupled to the ''Jordan-Fierz'' metric $\tilde{g}_{\mu\nu}=a^2(\varphi)g^*_{\mu\nu}$; all quantities with a tilde are related to this metric. That means that all nongravitational experiments measure this metric, although the field equations of the theory are better formulated in the Einstein metric. The indices of Einstein frame quantities are moved through Einstein metric, whereas those of Jordan-Fierz quantities are moved through Jordan-Fierz one. By varying S, one obtains

$$R^*_{\mu\nu}-\frac{1}{2}g^*_{\mu\nu}R^*=2\partial_\mu\varphi\partial_\nu\varphi-g^*_{\mu\nu}g_*^{\rho\sigma}\partial_\rho\varphi\partial_\sigma\varphi+\frac{8\pi G_*}{c^4}T^*_{\mu\nu}, \tag{2.2}$$

$$\Box_{g_*}\varphi=-\frac{4\pi G_*}{c^4}\alpha(\varphi)T_*, \tag{2.3}$$

where

$$T^{\mu\nu}_*=\frac{2}{\sqrt{-g_*}}\frac{\delta S_m}{\delta g^*_{\mu\nu}}, \tag{2.4}$$

$$\alpha(\varphi)=\frac{\partial\ln a(\varphi)}{\partial\varphi}, \tag{2.5}$$

and $\Box_{g_*}=g_*^{\mu\nu}\nabla^*_\mu\nabla^*_\nu$ is the Laplace-Beltrami operator of $g^*_{\mu\nu}$, ∇^*_μ denoting the Levi-Civita connection of $g^*_{\mu\nu}$. One can see that $\alpha(\varphi)$ is the basic, field-dependent coupling function between matter and scalar field. General relativity is obtained for $\alpha(\varphi)\to 0$.

The physical stress-energy tensor $\tilde{T}^{\mu\nu}=2(-\tilde{g})^{-1/2}\delta S_m/\delta\tilde{g}_{\mu\nu}$ is related to the Einstein-frame one by

$$T^\mu_{*\nu}=a^4(\varphi)\tilde{T}^\mu_\nu. \tag{2.6}$$

The equations of motion are given by the stress-energy balance equation, written in the Jordan-Fierz frame

$$\tilde{\nabla}_\nu\tilde{T}^\nu_\mu=0 \tag{2.7}$$

and in the Einstein frame

$$\nabla^*_\nu T^{\mu\nu}_*=\alpha(\varphi)T^*\nabla^\mu_*\varphi. \tag{2.8}$$

Finally, let us call φ_0 the cosmological value of the scalar field, which enters the theory as the boundary condition on the scalar field at spatial infinity.

B. Coordinates and variables

The present calculations have essentially been done by generalizing a previous work by Gourgoulhon [18] to tensor-scalar theory. Therefore, only a very brief presentation of coordinate and variable choice will be given here. The Einstein-scalar equations have been decomposed in the 3+1 formalism [19] onto a family of spacelike hypersurfaces Σ_t labeled by the real index t called the *coordinate time*. The *polar time slicing* has been chosen in order to have good singularity avoidance (see, e.g., [20] for discussion). On each hypersurface Σ_t the *radial gauge* has been chosen with spherical-like coordinates (r,θ,ϕ), since the considered problem is spherically symmetric. All these assumptions [spherical symmetry, radial gauge, and polar slicing (RGPS)] imply that the metric $g^*_{\mu\nu}=a^{-2}(\varphi)\tilde{g}_{\mu\nu}$ [which verifies Einstein-like equations (2.2), with an extra term] takes the diagonal form

$$ds^2=-N^2(r,t)dt^2+A^2(r,t)dr^2+r^2(d\theta^2+\sin^2\theta d\phi^2), \tag{2.9}$$

where $N(r,t)$ is called the *lapse function*. The metric $g^*_{\mu\nu}$ will often be described by the three functions $\nu(r,t)$, $m(r,t)$, and $\zeta(r,t)$ defined by

$$N(r,t)=\exp[\nu(r,t)], \tag{2.10}$$

$$A(r,t)=\left(1-\frac{2m(r,t)}{r}\right)^{-1/2}, \tag{2.11}$$

and

$$\zeta(r,t)=\ln\left(\frac{N}{A}\right). \tag{2.12}$$

All coordinates are expressed in the Einstein-frame, and asterisks are omitted. However, ''physical'' quantities will often be written in the Fierz metric and noted with a tilde.

In this work, neutron stars are modeled as self-gravitating perfect fluids. They can be considered to be made of degenerate matter at equilibrium, the equation of state being temperature independent (cold matter). This does not hold only soon after their formation. The stress-energy tensor is written as

$$\tilde{T}_{\mu\nu}=(\tilde{e}+\tilde{p})\tilde{u}_\mu\tilde{u}_\nu+\tilde{p}\tilde{g}_{\mu\nu}, \tag{2.13}$$

where $\tilde{u}_\mu$ is the four-velocity of the fluid, $\tilde{e}$ is the total energy density (including rest mass) in the fluid frame, and $\tilde{p}$ is the pressure. The relation to its Einstein-frame counterpart is $T^\mu_\nu=a^4(\varphi)\tilde{T}^\mu_\nu$. The description of the fluid is completed by an equation of state

$$\tilde{e}=\tilde{e}(\tilde{n}_B) \tag{2.14}$$

with $\tilde{n}_B$ being the baryonic density in the fluid frame. One then deduces the pressure as a function of $\tilde{n}_B$. Let Γ

$=n\tilde{N}\tilde{u}^0$ be the Lorentz factor connecting the fluid frame and Σ_t hypersurface frame, setting

$$\tilde{E}=-\tilde{T}_0^0$$

one gets

$$\tilde{E}=\Gamma^2(\tilde{e}+\tilde{p})-\tilde{p}. \tag{2.15}$$

The fluid baryonic number is represented by the *coordinate baryonic density*

$$\tilde{D}=\frac{\text{number of baryons in } \delta \mathrm{V}}{\delta \mathrm{V}}=A\Gamma\tilde{n}_B, \tag{2.16}$$

where $\delta V=r^2\sin\theta dr d\theta d\phi$ is the element of the coordinate three-volume on a given Σ_t, defined as the set of points whose coordinates are between r and $r+dr$, θ and $\theta+d\theta$, ϕ and $\phi+d\phi$. The fluid motion is described by the following variables:

$$V=\frac{dr}{dt}=\frac{u^r}{u^0}\ \text{(coordinate velocity)}, \tag{2.17}$$

$$U=\frac{\text{proper distance traveled on } \Sigma_t}{\text{elapsed proper time on } \Sigma_t}=\frac{A}{N}V. \tag{2.18}$$

One then has $\Gamma=(1-U^2)^{-1/2}$ and deduces the components of $\tilde{T}_{\mu\nu}$ given by Eq. (2.13). The fluid log enthalpy is also introduced, defined as

$$H=\ln\left(\frac{\tilde{e}+\tilde{p}}{\tilde{n}_B m_B c^2}\right) \tag{2.19}$$

and, finally, three ''scalar-field'' variables:

$$\eta=\frac{1}{A}\frac{\partial\varphi}{\partial r}, \tag{2.20}$$

$$\psi=\frac{1}{N}\frac{\partial\varphi}{\partial t}, \tag{2.21}$$

$$\Xi=\eta^2+\psi^2. \tag{2.22}$$

C. Tensor-scalar field equations

Spherical symmetry helps to obtain gravitational field equations; we followed the procedure described by Gourgoulhon [18], projecting Eqs. (2.2),(2.3) on the three-surfaces Σ_t and along their normal. Hereafter, we use the following notation:

$$q_\pi=\frac{8\pi G_*}{c^4}.$$

The tensor Einstein-like equations (2.2) then turn into one Hamiltonian constraint equation

$$\frac{\partial m}{\partial r}=r^2\frac{c^2}{2G_*}(\Xi+q_\pi a^4(\varphi)\tilde{E}), \tag{2.23}$$

three momentum constraint equations which reduce to only one nonvanishing equation,

$$\frac{\partial m}{\partial t}=r^2\frac{c^2}{2G_*}\left[2\frac{N}{A}\psi\eta-q_\pi a^4(\varphi)(\tilde{E}+\tilde{p})V\right], \tag{2.24}$$

and six Einstein dynamical equations which here reduce to two nonvanishing equations, one of which degenerate, only giving a condition on the lapse function

$$\frac{\partial\nu}{\partial r}=\frac{q_\pi A^2}{2}\left[\frac{mc^2}{4\pi r^2}+a^4(\varphi)r(\tilde{p}+U^2(\tilde{E}+\tilde{p}))+r\Xi\right]. \tag{2.25}$$

The other one will not be used in this work.

Writing the scalar-field wave equation (2.3) with our variables gives

$$\frac{\partial^2\varphi}{\partial t^2}=e^{2\xi}\left(\Delta\varphi+\frac{\partial\xi}{\partial r}\frac{\partial\varphi}{\partial r}\right)+\frac{\partial\xi}{\partial t}\frac{\partial\varphi}{\partial t}-q_\pi\frac{\alpha(\varphi)a^4(\varphi)N^2}{2}\times[\tilde{E}-3\tilde{p}-(\tilde{E}+\tilde{p})U^2]. \tag{2.26}$$

One more equation concerning the scalar field will be used; although it is redundant with Eqs. (2.23)–(2.26), from which it is deduced, it will be useful for numerical integration:

$$\frac{1}{2}\frac{\partial\Xi}{\partial t}=\left\{\frac{N}{A}\left[\psi\Delta\varphi+\eta\frac{\partial\psi}{\partial r}\right]+\frac{2N}{A}\psi\eta\frac{\partial\nu}{\partial r}-\Xi\frac{G_*A^2}{rc^2}\frac{\partial m}{\partial t}\right\}+\psi q_\pi\alpha(\varphi)a^4(\varphi)N[\tilde{E}-3\tilde{p}-(\tilde{E}+\tilde{p})U^2]. \tag{2.27}$$

D. Matter evolution equations

In order to get the evolution of the variables $\tilde{E}$ and U, let us consider the momentum-energy conservation equation (2.8). We get

$$\frac{\partial\tilde{E}}{\partial t}+\frac{1}{r^2}\frac{\partial}{\partial r}(r^2(\tilde{E}+\tilde{p})V)=-(\tilde{E}+\tilde{p})\{\alpha(\varphi)N[(3+U^2)\psi+4U\eta]+rAN[(1+U^2)\psi\eta+U\Xi]\}, \tag{2.28}$$

$$\frac{\partial U}{\partial t}+V\frac{\partial U}{\partial r}=-\frac{1}{\tilde{E}+\tilde{p}}\left(U\frac{\partial\tilde{p}}{\partial t}+\frac{N}{A}\frac{\partial\tilde{p}}{\partial r}\right)-\frac{AN}{\Gamma}\left[\frac{G_*m}{r^2c^2}+q_\pi a^4(\varphi)\frac{r\tilde{p}}{2}+\frac{\alpha(\varphi)}{A}(\eta+U\psi)+rU\eta\psi+\frac{r}{2}\Xi\right]. \tag{2.29}$$

Equation (2.28) expresses the total energy conservation (matter plus gravitational and scalar energy), Eq. (2.29) being the tensor-scalar analogous of the Euler equation. One notes that in the latter, the $1/(\tilde{E}+\tilde{p})[U(\partial\tilde{p}/\partial t)+(N/A)(\partial\tilde{p}/\partial r)]$ term which may cause some trouble when numerically calculating it, since it is the quotient of two

quantities vanishing at the surface of the star. Thus, if one uses the log enthalpy (2.19), this term may be replaced by $1/\Gamma^2[U(\partial H/\partial t)+(N/A)(\partial H/\partial r)]$, which is well defined near the surface.

Expressing the baryonic number conservation

$$\widetilde{\nabla}_\mu \widetilde{n}_B \widetilde{u}^\mu = 0 \tag{2.30}$$

one obtains

$$\frac{\partial \widetilde{D}}{\partial t} + a(\varphi)\frac{1}{r^2}\frac{\partial}{\partial r}(r^2 \widetilde{D} V) + \alpha(\varphi)\widetilde{D} N(3\psi + 4U\eta) = 0. \tag{2.31}$$

Because log enthalpy is used in order to avoid numerical singularities at the surface, there has to be an evolution equation of that quantity. Since $H=H(\widetilde{n}_B)$, and $\widetilde{n}_B=\widetilde{D}/A\Gamma$, one may write

$$\begin{aligned}\frac{\partial H}{\partial t} + V\frac{\partial H}{\partial r} &= \frac{\partial H}{\partial \widetilde{n}_B}\left(\frac{\partial \widetilde{n}_B}{\partial t} + V\frac{\partial \widetilde{n}_B}{\partial r}\right) \\ &= \frac{\partial H}{\partial \widetilde{n}_B}\frac{V}{A\Gamma}[1-a(\varphi)]\frac{\partial \widetilde{D}}{\partial r} - \widetilde{n}_B\frac{\partial H}{\partial \widetilde{n}_B} \\ &\quad \times\left[\frac{1}{r^2}\frac{\partial}{\partial r}(r^2 V) + \alpha(\varphi)N(3\psi+4U\eta)\right. \\ &\quad \left. + \frac{1}{A}\left(\frac{\partial A}{\partial t} + V\frac{\partial A}{\partial r}\right) + \Gamma^2 U\left(\frac{\partial U}{\partial t} + V\frac{\partial U}{\partial r}\right)\right],\end{aligned} \tag{2.32}$$

with terms in the right-hand side being replaced using Eqs. (2.23), (2.24), and (2.29) by source terms involving $\widetilde{E}, \widetilde{p}$ and Ξ. The results of numerical integration of all these equations (2.23)–(2.32) will be presented in the next section.

III. NUMERICAL RESULTS

The numerical procedure, the code, and its tests are described in the Appendix. In this section, only results are presented and discussed. An important choice is that of the coupling function $a(\varphi)$. Following [12], we chose a function depending on two parameters for all of our study:

$$a(\varphi) = e^{\alpha_0(\varphi-\varphi_0)+(\beta_0/2)(\varphi-\varphi_0)^2}. \tag{3.1}$$

Figure 9 of [12] gives constraints on the (α_0,β_0) space of parameters, imposed by binary-pulsar measurements. Section III D investigates this space of parameters for scalar gravitational waves. Note that Brans-Dicke theory is obtained for $\beta_0=0$.

A. Static configurations

Physical scenarios to form a black hole involve either an accreting neutron star or a post-supernova remnant (when a part of the ejected envelop falls back onto the new-born neutron star). In both cases, the mass of the neutron star must reach its maximal value above which the star becomes unstable. It is then interesting to get unstable equilibrium configurations of neutron stars, endowed with a scalar field, close to the maximal mass. They are used as initial configurations for the collapse. Thus, setting all $\partial/\partial t$ terms to zero, as well as V and U in Eqs. (2.23)–(2.28), one gets the scalar equivalent of the Tolman-Oppenheimer-Volkoff (TOV) system. The system obtained is the same as Eqs. (7) in [11], since the same gauge is used. Considering a polytropic equation of state

$$\begin{aligned}\widetilde{e}(\widetilde{n}_B) &= \widetilde{n}_B\widetilde{m}_B + K\frac{\widetilde{n}_0\widetilde{m}_B}{\gamma-1}\left(\frac{\widetilde{n}_B}{\widetilde{n}_0}\right)^\gamma, \\ \widetilde{p} &= K\widetilde{n}_0\widetilde{m}_B\left(\frac{\widetilde{n}_B}{\widetilde{n}_0}\right)^\gamma,\end{aligned} \tag{3.2}$$

with $\widetilde{m}_B = 1.66\times10^{-27}$ kg and $\widetilde{n}_0 = 0.1$ fm^{-3}, one can integrate the scalar TOV system, starting at the center with a given value for $\widetilde{n}_B(r=0)$, up to the surface at which $\widetilde{n}_B(r=R_{\rm star})=0$. In this study, two types of polytrope will be used: (1) $\gamma=2.34$ and $K=0.0195$, which has already been used by [11] to fit equation of state II (EOSII) in [21], called EOS1 in this paper; (2) $\gamma=2$ and $K=0.1$, as used in [22], called EOS2 in this paper. Then for each static configuration, the total Arnowitt-Deser-Misner (ADM) mass of $g^*_{\mu\nu}$, which will be called the gravitational mass and the total scalar charge ω such that, for $r\to\infty$, $\varphi(r)=\varphi_0+G_*\omega/r+O(1/r^2)$, can be determined through Eqs. (8) of [11]. These two quantities are useful to match the obtained interior solution to the exterior one (spherically symmetric solution in vacuum), which is known analytically in another gauge (described in [23]) and thus one can obtain a static solution everywhere. The resulting fields are shown in Fig. 1 for $\beta_0=-6$, with large value of the scalar field inside the star, even for a very small asymptotic field φ_0 (spontaneous scalarization). These solutions are then used as initial values for the dynamical evolution. They have been computed, with increasing central densities $\widetilde{n}_B(r=0)$, in order to get an ''unstable'' configuration (for which gravitational mass is a decreasing function of the density). This property is not evident in tensor-scalar theory, but the dynamical code being sensitive enough to trigger the instability only by round-off errors, it has been checked numerically. The hydrostatic equilibrium is obtained, thanks to pseudospectral techniques (see Appendix 1 and [24]), up to very high accuracy (10^{-10} relative error on the hydrostatic equilibrium), which enables the dynamical code to be sensitive to instability (see [18]).

B. Scalar gravitational waves

Hereafter, four collapse calculations will be presented, called A, B, C, and D. The parameters of the static configurations, which were used as initial conditions for the collapses, are described in Table I. Note that collapses A and B use a $\gamma=2.34$ polytrope, whereas C and D use a $\gamma=2$ one. First, only the case A will be considered. As far as the hydrodynamic part is concerned, the collapse is very similar to that in general relativity, described in [18]. It can be seen from Fig. 2, that $A[t,R_{\rm star}(t)]\to\infty$ due to the pathological behavior of the radial gauge when $R_{\rm star}$ is approaching the Schwarzschild radius. An apparent horizon is expected to

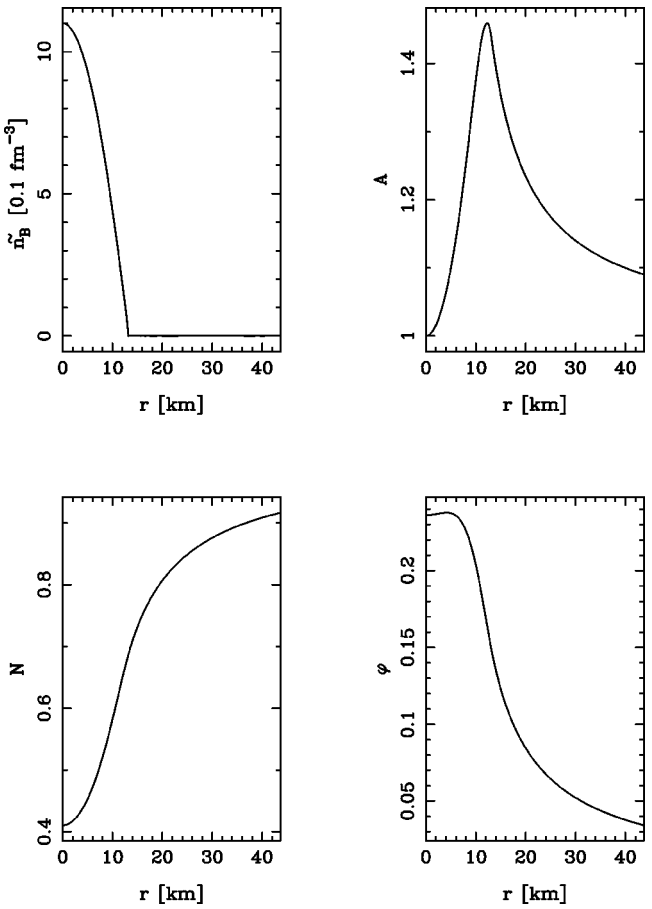

FIG. 1. Density ($\tilde{n}_B$), metric potentials (A and N), and scalar field (φ) profiles for a neutron star of $2.4M_\odot$, for EOS1 ($\gamma=2.34$ and $K=0.0195$ polytrope) and with a coupling function $a(\varphi)=\exp(-3\varphi^2)$. The asymptotic scalar field value is $\varphi_0=10^{-5}$. Star's radius $R_{\rm star}=13.1$ km.

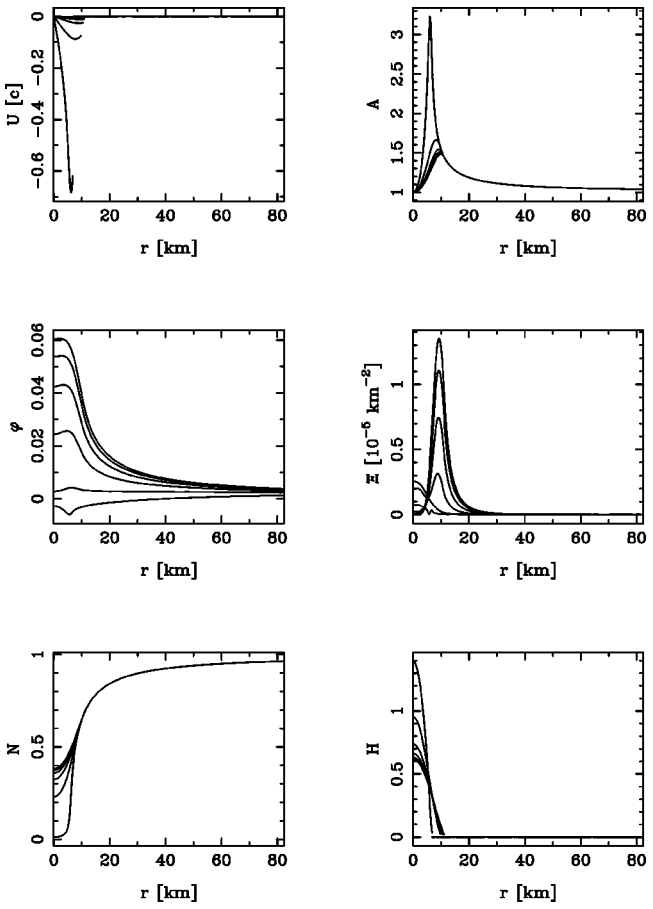

FIG. 2. Profiles of various quantities at different values of t between 0 and 4.64 ms, for collapse A. The fluid velocity $U(r,t)$, measured by the hypersurface observer, is expressed in units of c and its evolution is downward, the extremity of each curve giving the position of the star's surface at the corresponding instant. The evolution for $A(r,t)$ (metric potential), $\Xi(r,t)$ (scalar ''energy'') and $H(r,t)$ (log-enthalpy) is upward, and downward for $\varphi(r,t)$ (scalar field) and $N(r,t)$ (lapse).

develop, but minimal two-surfaces cannot be described by the radial gauge. On Fig. 2 are plotted several quantities during the collapse [until $N(r=0)$ becomes too small]. Thus, although RGPS coordinates are not well adapted for the description of a black hole, they were used to describe the collapse toward it, as in [18]. Moreover, from Figs. 2 and 3 one sees that the star has almost entered its Schwarzschild radius ($R_{\rm star}/R_{\rm Schwarzschild}=1.001$ at the end of the collapse); so that no significant later evolution could be achieved inside the star. Actually, one notices that the lapse goes to zero within the Schwarzschild radius of the star. Since all evolution equations are written $\partial/\partial t=N\times$(source term) and the coordinate velocity $V=(N/A)U\to 0$, all hydrodynamic and scalar-field quantities are ''frozen'' inside the star. Therefore, their evolution can be numerically stopped, in order to avoid the singularity of $A(r=R_{\rm star})$. However, all field quantities continue to evolve *outside* the star as long as one wants in terms of coordinate time (which is the time of an observer at spatial infinity).

TABLE I. Initial condition parameters of the collapses presented in this paper. The equations of state (EOS) are described in Sec. III A, φ_0 is the asymptotic scalar field value (given by cosmological evolution), α_0 and β_0 are the coupling function parameters (3.1), $R_{\rm star}$ denotes star's radius, $\tilde{n}_B(r=0)$ is the central baryon density (in units of nuclear density, 1 $n_{\rm nuc}=10^{44}$ m^{-3}), M_G is the $g^*_{\mu\nu}$-frame ADM mass, M_B the baryonic one, and ω the scalar charge.

Collapse	EOS	φ_0	α_0	β_0	$R_{\rm star}$ [km]	$\tilde{n}_B(r=0)$ [$n_{\rm nuc}$]	M_G [$M_\odot$]	M_B [$M_\odot$]	ω [$M_\odot$]
A	1	10^{-5}	5×10^{-5}	-5	11.2	10.4	1.97	2.26	0.204
B	1	10^{-5}	2.5×10^{-2}	-5	11.8	10.4	2.07	2.41	0.484
C	2	10^{-5}	5×10^{-5}	-5	21.5	4	3.31	3.68	0.921
D	2	10^{-5}	2.5×10^{-2}	-5	22.2	4	3.41	3.82	1.16

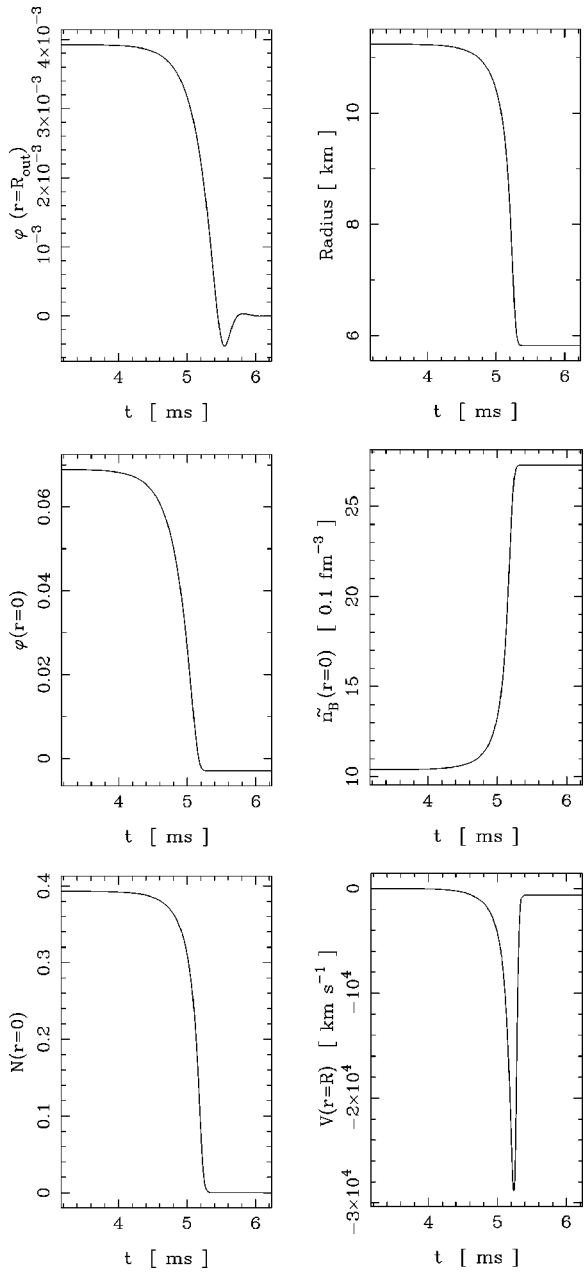

FIG. 3. Evolutions of various quantities during the collapse A, as a function of the coordinate-time t. $R_{\rm out}=300$ km is the radius of the outer edge of the grid. $\varphi(r,t)$ is the scalar field and the radius is the coordinate value for which $\tilde{n}_B$, the baryon density is zero. $N(r=0)$ is the lapse at star's center and $V(r=R)$ is the star's surface velocity.

The results of this evolution are shown in Fig. 3, for collapse A. The fate of the scalar field is particularly interesting: for $r\gg R_{\rm star}$ the field relaxes toward the asymptotic constant value set by cosmological evolution; the scalar energy of the star is radiated away as scalar gravitational wave. The scalar field $[\varphi(r=R_{\rm out})]$ is considered to be sufficiently far away from the star (i.e., in the wave zone) to give the monopolar gravitational wave signal. Using the ''frozen star'' to evolve the fields outside the star, makes the integration time long enough to get all the information from the collapse at $r\gg R_{\rm star}$ (where all gauges become equivalent). The main difference from general relativity is the scalar monopolar radiation, which carries away energy and can interact with a detector. Looking far from the source (at a distance $r\gg R_{\rm star}$), one can write the metric (see [1])

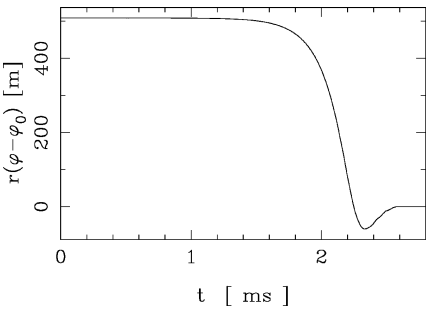

FIG. 4. Wave form of the emitted signal during collapse B. The plotted quantity is the function $F(t)$ (see Sec. III B), measured at $r=300$ km and expressed in meters. $\varphi(r,t)$ is the scalar field and φ_0 its asymptotic value. To get the gravitational wave amplitude h, one must use Eq. (3.4).

$$\tilde{g}_{\mu\nu}(r,t)=a^2(\varphi_0)\left[f_{\mu\nu}+\frac{1}{r}(h_{\mu\nu}+2\alpha_0 F f_{\mu\nu})+O(r^{-2})\right], \tag{3.3}$$

where $f_{\mu\nu}$ is the flat metric and $h_{\mu\nu}(t-r/c)$ and $F(t-r/c)$ are, respectively, the quadrupolar and monopolar components of the wave. Since this work is done in spherical symmetry, only the monopolar mode shall be considered. The

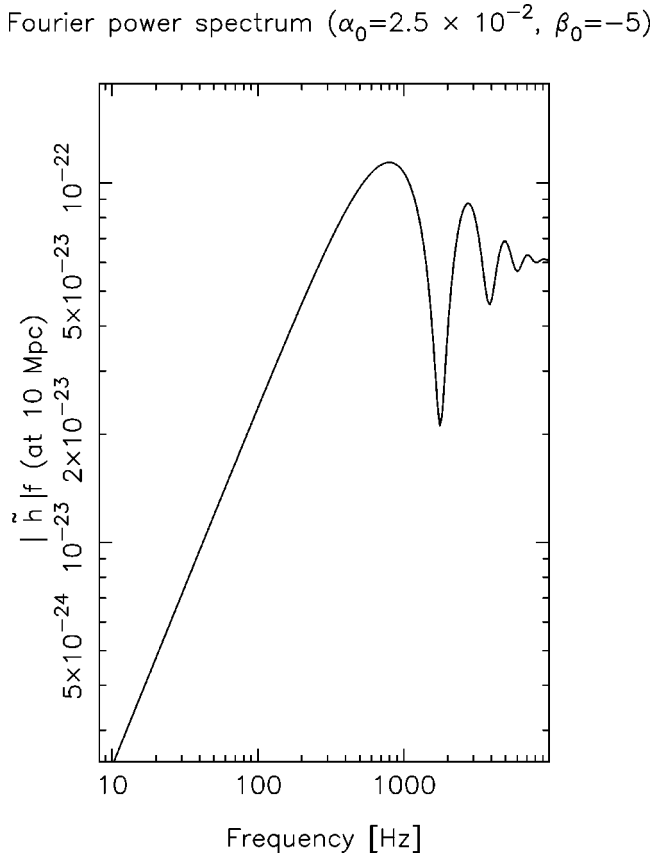

FIG. 5. Fourier power spectrum of the scalar gravitational wave emitted during collapse B. $\tilde{h}$ is the Fourier transform of the signal, measured at 10 Mpc and f, the frequency.

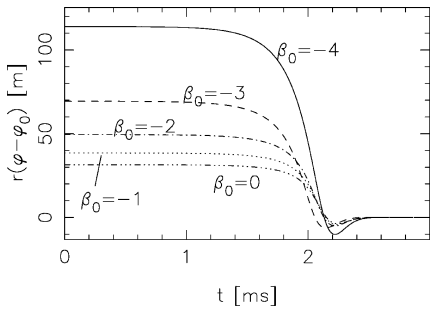

FIG. 6. Same as Fig. 4 but for different collapses. $\alpha_0=3.16\times10^{-2}$ for all of them, but β_0 varies from -4 (upper curve, —) to $\beta_0=0$ (lower curve, -·· · ·-).

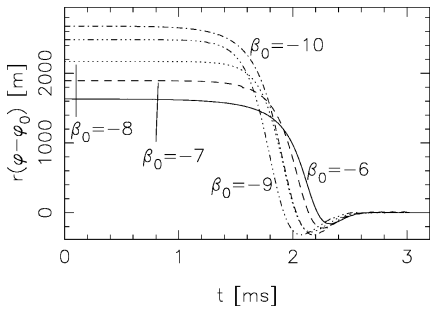

FIG. 7. Same as Fig. 6 but β_0 varies from -10 (upper curve, - · -) to $\beta_0=-6$ (lower curve, —).

function F is the same as that of Eq. (A3), and is plotted for collapse B in Fig. 4. If one wants to compare the amplitude to those of general relativistic gravitational waves (h_{ij}^{TT}), at a distance d, then the right quantity is (see [1], [17], or [25]):

$$h(t)=\frac{2}{d}a^2(\varphi_0)\alpha_0 F(t). \tag{3.4}$$

The Fourier spectrum of the signal is

$$\tilde{h}(f)=\int_0^{t_{\max}} h(t)e^{2\pi i f t}dt \tag{3.5}$$

and the power spectrum ($f|\tilde{h}|$), which is plotted in Fig. 5 for the collapse B, is then useful to determine the characteristic frequency f_c of the signal. Actually, the quantity to be compared with detectors' sensitivity is

$$\tilde{h}_c=|\tilde{h}(f_c)|\sqrt{f_c}, \tag{3.6}$$

which is expressed in $\mathrm{Hz}^{-1/2}$. From Fig. 5, one sees that a ''collapse B'' could be detected by VIRGO, provided it occurs within 300 kpc. Finally, the radiated Einstein-frame Bondi energy is written as

$$E_{\mathrm{scal}}=\frac{c^3}{G_*}\int_0^{+\infty}\left(\frac{dF}{dt}\right)^2 dt \tag{3.7}$$

which is the total energy radiated in gravitational waves.

C. Comparison with previous works

Because all previous works have studied an Oppenheimer-Snyder collapse, for comparison some runs were done putting $\tilde{p}$ and H to zero.

The first work by Shibata *et al.* [15] considered the dust collapse in the Brans-Dicke theory ($\beta_0=0$). The authors used two types of initial conditions, called (A) and (B). The case (A) starts the collapse with $\varphi=\varphi_0$, whereas (B) starts it with a quasistatic solution for φ. Making the same dust collapses, the same wave forms and amplitudes were obtained (their Φ is related to φ by $\Phi=2\ln[A(\varphi)]=2\alpha_0(\varphi-\varphi_0)$). Taking the equation of state into account, with equilibrium initial configurations (which are the most realistic possible), gives the wave form of Fig. 6 ($\beta_0=0$). The form and amplitude are very close to the (B) type collapses of Shibata *et al.* (see their Fig. 3), the power spectra being close too (Fig. 5, with lower amplitude, and Fig. 6 of [15]).

Another work in Brans-Dicke theory, with dust matter, was done by Scheel *et al.* [16], dealing more with the fate of the final object. However, comparing $2\alpha_0 dF/dt$ of this work, with f' of their paper gives the same result. Whereas the authors can conclude on the final state of the collapse, this work cannot describe it. All that can be said is that the scalar charge (or mass) is all radiated away, so that the scalar field relaxes toward its cosmological value, and that an apparent horizon is *expected* to appear (cf. Sec. III B). These results still hold in more general tensor-scalar theory. Finally, it can be pointed out that, contrary to their work, here the tensor mass in the *Einstein* frame is considered, not in the Jordan-Fierz one.

The last study of spherically symmetric collapse in tensor-scalar theory was done by Harada *et al.* [17]. They used the Oppenheimer-Snyder metric (in general relativity) as a background spacetime and did some Taylor expansion of tensors and equations in terms of scalar field coupling function parameters. Therefore, they used unrealistic initial conditions ($\varphi=\varphi_0$) and could not study the cases of spontaneous scalarization. Wave forms resulting from our calculations for different β_0, from -10 to 50 are shown in Figs. 6 to 9, with unstable equilibrium initial configurations and full hydrodynamics. $\alpha_0=3.16\times10^{-2}$ as in [17] and the mass is the maximal one (cf. Sec. III A), the ratio $R_{\mathrm{star}}/M\simeq4$. The results are different, although showing the same tendancy as in [17], for many β_0, due to the fact that Harada *et al.* took unrealistic initial conditions. Thus in their simulations, when the collapse begins the scalar field, on the one hand, evolves to reach its quasiequilibrium configuration, on the other hand, it feels the effects of the collapse. Their signal is then a superposition of these two effects: a raise of the scalar field up to its equilibrium value, with one or several oscillations de-

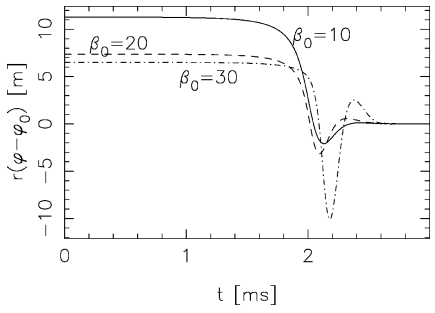

FIG. 8. Same as Fig. 6 but β_0 varies from 10 (upper curve, —) to $\beta_0=30$ (lower curve, - · -).

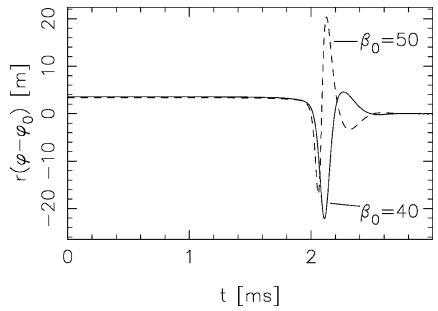

FIG. 9. Same as Fig. 6 but $\beta_0=40$ (—) and $\beta_0=50$ (---).

pending on β_0, then the fall of this field, due to the collapse of the matter. The signals for $\beta_0>20$ have more important oscillations than other ones; this may be explained as follows. Inside the star, there are unstable modes which develop for these β_0 and when the ratio R/M becomes small, as it has been shown by Harada in for static configurations (see Fig. 5 of [26]). This is due to the fact that, near the star's center, $\widetilde{E}-3\widetilde{p}<0$ allowing for spontaneous scalarization to develop.[2] Here, one can see an effect of the pressure on the signal. These nonperturbative modes develop on a time scale τ:

$$\tau\sim\frac{\tau_{\rm ff}}{\sqrt{|\beta_0|}}$$

(see Eq. (5.3) of [26]) with $\tau_{\rm ff}$ being the free-fall time of the star. Thus, for $\beta_0>20$ the modes develop during the collapse, when R/M becomes small enough. This rise is fast enough to be (at least partly) seen before the star enters its Schwarzschild radius (see Figs. 8 and 9).

D. Exploring the parameter space

Thanks to the fact that it solves complete equations, the code presented in this paper is able to explore a larger part of the parameter space and give more ''physical'' results. In Sec. III C β_0 has been varied from -10 to 50 and α_0 was fixed. The effect of spontaneous scalarization, for $\beta_0\simeq-5$ and lower, was observed changing the amplitude, but not the shape of the wave. However, the two regimes (depending on the value of β_0) were studied separately, when varying α_0. This latter has been taken between 0 and 3×10^{-2}, either in spontaneous scalarization ($\beta_0=-6$), or without it ($\beta_0=-4$). The results are shown in Fig. 10 for $\widetilde{h}_c$ and in Fig. 11 for $E_{\rm scal}$. One notices that for $\beta_0=-6$ $\widetilde{h}_c\propto\alpha_0$ and $E_{\rm scal}\propto$const, whereas both $\propto\alpha_0^2$ for $\beta_0=-4$. The scalar field amplitude does (almost) not depend on α_0 in spontaneous scalarization, whereas it is directly proportional to it otherwise, as in Brans-Dicke theory.

The equation of state has also been changed. Collapses C and D have been performed with EOS2 (see Sec. III A). Results are shown in Fig. 12 for collapse D and are similar to those of EOS1 (collapse B), the scalar gravitational wave signal having the same shape shifted since f_c is higher (1 kHz for D, versus 800 Hz for B). This difference, as well as

[2]See the simplified model of [11].

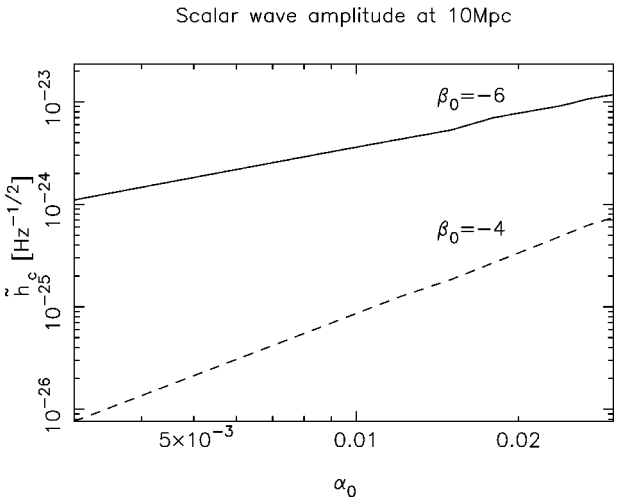

FIG. 10. Amplitude of the scalar gravitational wave $\widetilde{h}_c$ [see Eq. (3.6)], at 10 Mpc, as a function of the coupling coefficient α_0, for two different values of β_0.

that in amplitude, can easily be explained by the change of the mass of the unstable-equilibrium configuration. Thus, varying the parameters of the polytropic equation of state is not of much interest. The use of a realistic equation of state would be better (as in [18]) but, for this work, a polytrope gives already good results.

Finally, a few more runs were performed with EOS1 varying β_0 from 50 to -10 and, for each β_0, the maximal value of α_0 allowed by solar-system experiments (see, e.g., Fig. 9 of [12]) was taken. More precisely, the lowest value of

$$\alpha_0^2<10^{-3}$$

and

$$\alpha_0^2<\frac{1.2}{|\beta_0|}\times10^{-3} \tag{3.8}$$

was taken. Results are shown in Figs 13 and 14 for $E_{\rm scal}$, and it can be seen that effects of spontaneous scalarization appear for $\beta_0<-4.4$ and that for $\beta_0>20$, one can see effects of

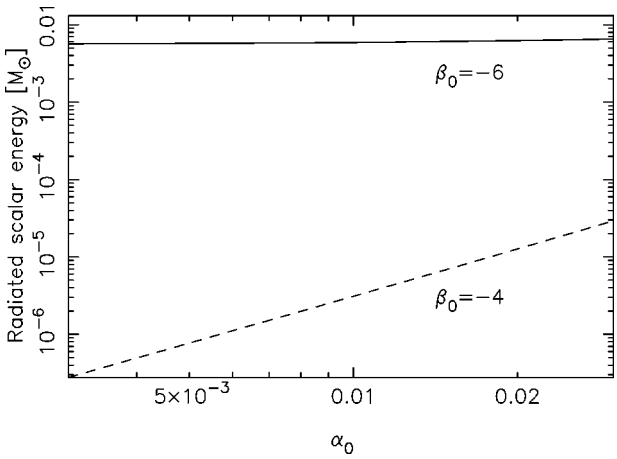

FIG. 11. Radiated scalar gravitational energy $E_{\rm scal}$ [see Eq. (3.7)] emitted during a collapse, as a function of the coupling coefficient α_0, for two different values of β_0.

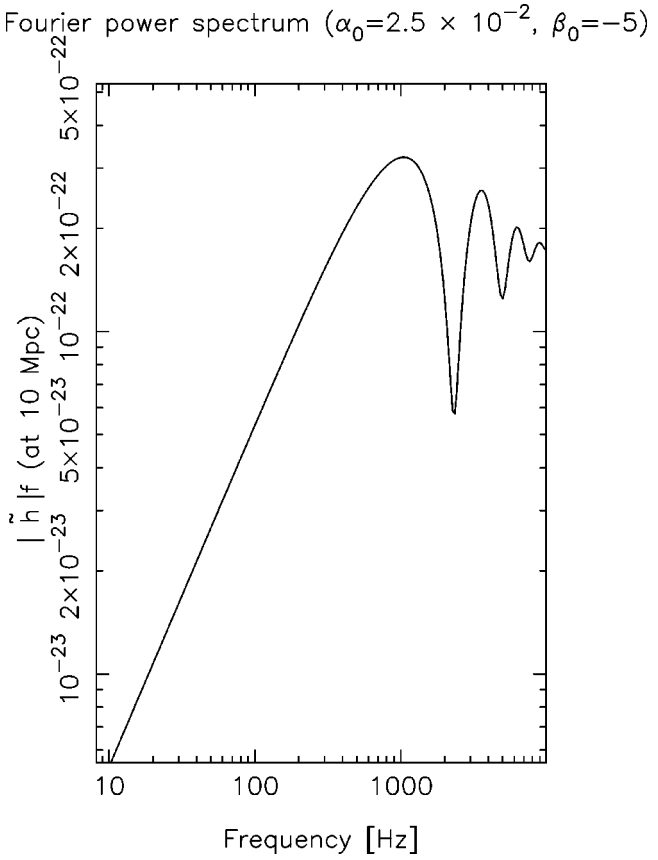

FIG. 12. Same as Fig. 5, but for collapse D.

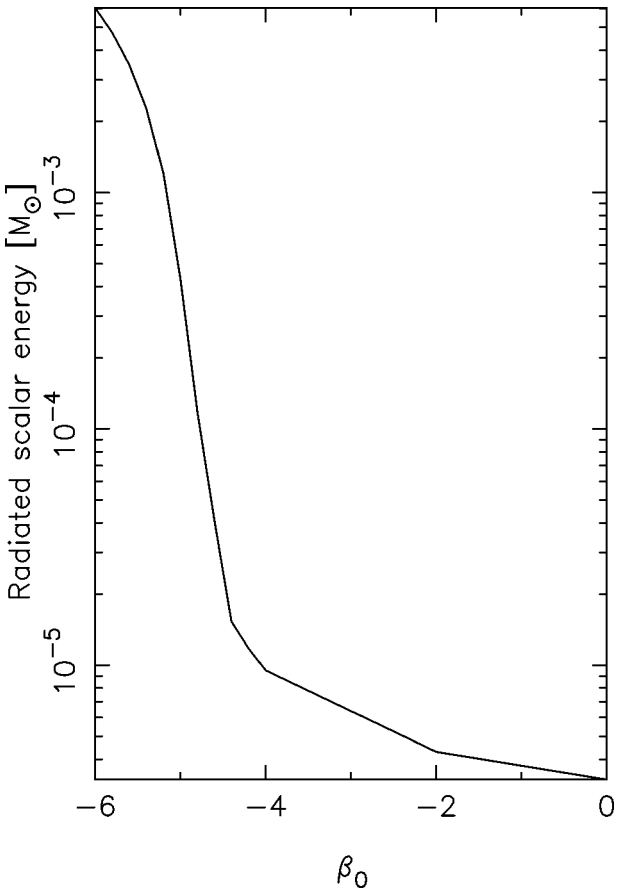

FIG. 13. Radiated scalar gravitational energy $E_{\rm scal}$ [see Eq. (3.7)] emitted during a collapse, as a function of the coupling coefficient β_0, between -6 and 0. For each β_0, α_0 has the maximal value, imposed by solar-system experiments [see Eq. (3.8)].

instabilities of the scalar field (see Sec. III C). As far as the gravitational wave signal is concerned, the quantity plotted in Figs. 15 and 16 is $\tilde{h}_c$, at 10 Mpc from the source. The characteristic frequency range is 700 Hz$\leqslant f_c \leqslant$900 Hz except for $\beta_0 \geqslant 20$, where $f_c \sim 2000$ Hz. The maximal signal $\tilde{h}_c \simeq 5\times10^{-24}$ at 10 Mpc which is, at least, one order of magnitude lower than the best expected sensitivity of interferometric detectors currently under construction (see e.g. [27]). However, one may compare the signal amplitude and energy to those of similar collapses in general relativity (two- and three-dimensional stellar core collapse, see [28] and [29]) and see that both are quite higher. Thus, if spontaneous scalarization effects are likely to occur, their gravitational signal should be more easily detected than the quadrupolar one from a collapsing source (an aborted supernova or neutron star reaching its maximal mass by accretion).

IV. CONCLUSIONS

This work has been done with very few approximations [$A\times N$ set to a constant at the outer edge of the grid, see Eq. (A6) and Appendix 3, and evolution ''frozen'' when the lapse becomes too small]; all the tensor-scalar equations, including hydrodynamics, were solved with high accuracy by means of spectral methods. Although the gauge choice does not allow any study of the state of the final object, the scalar gravitational wave signals can be obtained and the results compare well with previous (simplified) works. From that comparison it can be said that, whereas taking pressure into account, in most cases, does not have significant effects on the signal (which had to be demonstrated), it is the only way to get reliable initial conditions and to trigger the collapse in a ''natural'' way. Doing so helps to get clean wave forms. On the other hand, since the complete set of tensor-scalar equations was solved, it was possible to study the effects of coupling function parameters. Mainly, one sees that the outgoing monopolar gravitational wave is very dependent on the coupling function, especially the β_0 parameter. This is interesting because the α_0 parameter can be constrained by solar-system experiments, since it represents only a linear deviation from general relativity, whereas β_0 cannot be really probed in that way. Even if the signal from extragalactic sources is not strong enough to be detected, it is higher than the quadrupolar one and involves more energy. This means that if a quadrupolar wave signal is detected by VIRGO or LIGO with no monopolar component, then the constrain on tensor-scalar theory will be quite strong. A future study is the supernova collapse and bounce in this framework since, in that case, one has electromagnetic and neutrino signals which make the use of even negative results of detection possible.

ACKNOWLEDGMENTS

I thank Thibault Damour for suggesting this work, for fruitful discussions, and a critical reading of the manuscript. I am very grateful to Eric Gourgoulhon for help, discussions,

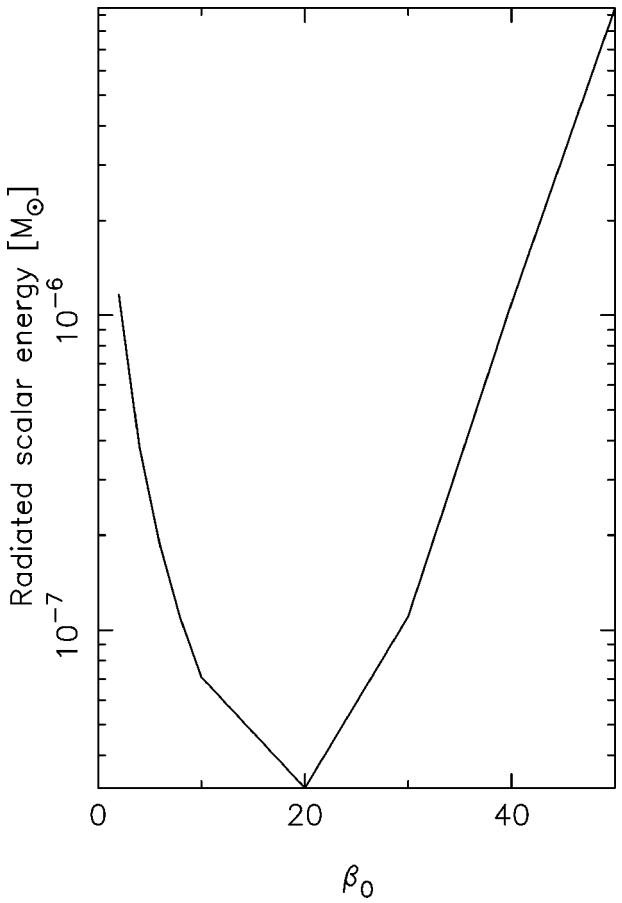

FIG. 14. Same as Fig. 13 but β_0 varies from 0 to 50.

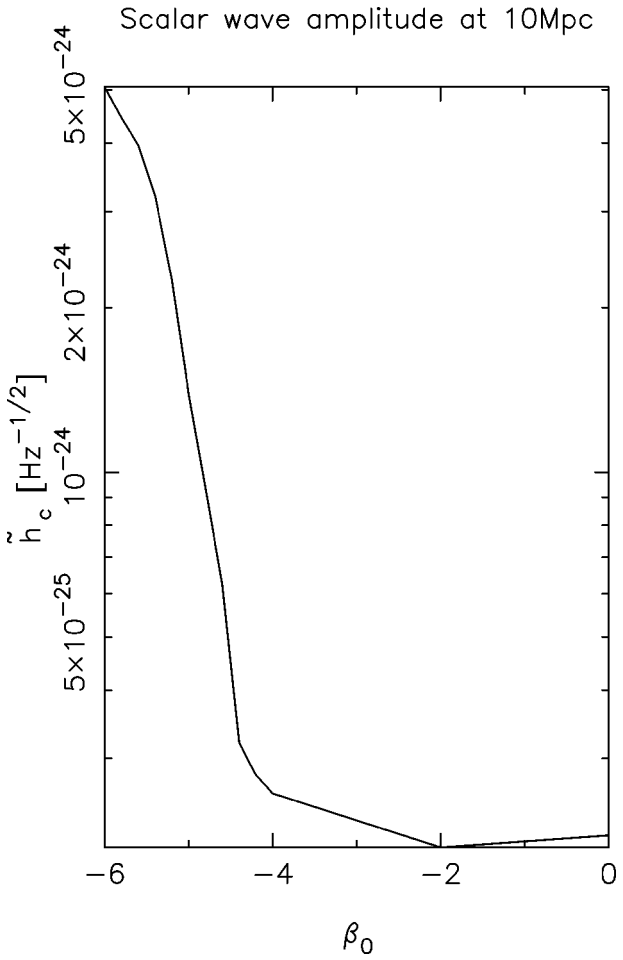

FIG. 15. Amplitude of the scalar gravitational wave $\tilde{h}_c$ [see Eq. (3.6)], at 10 Mpc, as a function of the coupling coefficient β_0, between -6 and 0. For each β_0, α_0 has the maximal value, imposed by solar-system experiments [see Eq. (3.8)].

and a careful reading of the manuscript. The numerical calculations have been performed on Silicon Graphics workstations purchased thanks to the support of the SPM department of the CNRS and the Institut National des Sciences de l'Univers.

APPENDIX: NUMERICAL PROCEDURE

Hereafter, some details of the numerical techniques (spectral methods) are described. More complete explanations can be found in [24], [30], and [31].

1. Chebyshev decomposition

The numerical problem is to solve a set of partial differential equations. For this purpose, each field (or function) $f_{t_0}(r)$ is represented, at a given time t_0, as a truncated series of Chebyshev polynomials (or as a column vector of the coefficients of this series). The usual number of coefficients (or points) is between 17 and 65. Then all spatial operators such as

$$f \to \frac{\partial f}{\partial r},\ \int f,\ \frac{1}{r} f,\ rf,\ \Delta f$$

reduce to matrix multiplications of the set of f's coefficients. Constraint equations (2.23) and (2.25) are thus easily integrated. Other operations, such as the multiplication of two functions, must still be done in the physical space (at grid's points).

Evolution equations are written in the form

$$\left.\frac{\partial f}{\partial t}\right|_{t=t_{J+1/2}} = \frac{f_{t_{J+1}} - f_{t_J}}{t_{J+1} - t_J} = \mathcal{S}(f)_{t_{J+1/2}} \tag{A1}$$

with $\mathcal{S}$ being a spatial operator on f and t_J being the Jth instant of integration. There is need to evaluate $\mathcal{S}$ at time $t_{J+1/2}$, which can be done either explicitly (extrapolated from known quantities at t_J and t_{J-1}) or implicitly (interpolated from unknown quantity at t_{J+1}). Explicit integration suffers from the severe Courant-Friedrich-Levy constraint on the time step. However, in the case of an advection equation [such as Eq. (2.31)], it can be used almost with an arbitrary time step provided that the advection velocity is zero at the edges of the grid; hence the *comoving* grid with the fluid (see Appendix 3). The implicit way requires us to write

$$\left(1 - \frac{(t_{J+1} - t_J)}{2}\mathcal{S}\right) f_{t_{J+1}} = f_{t_J} + \frac{(t_{J+1} - t_J)}{2}\mathcal{S}(f_{t_J}), \tag{A2}$$

where the function f is represented by its coefficients and with $\{1 - [(t_{J+1} - t_J)/2]\mathcal{S}\}$ being a matrix, which is inverted to get the solution $f_{t_{J+1}}$. In the case where one has to impose boundary conditions, the right-hand side of Eq. (A2) is re-

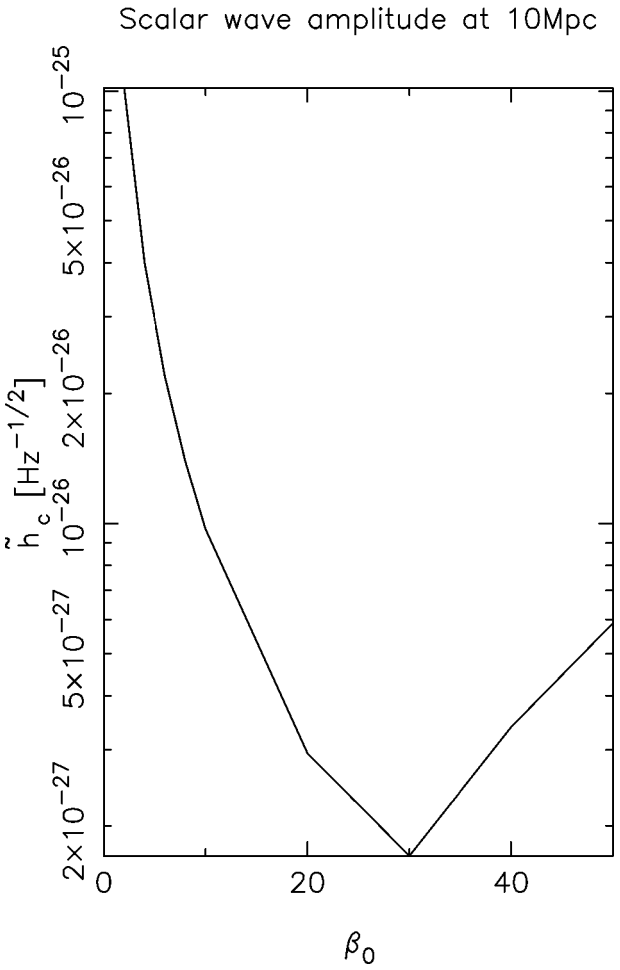

FIG. 16. Same as Fig. 15 but β_0 varies from 0 to 50.

placed by a vector of coefficients containing zeros except on the last or last but one column. One thus gets a ''free'' solution which can be combined with the first one in order to satisfy boundary conditions.

2. Wave equation

Unfortunately, the $\mathcal{S}$ operator present in Eq. (A1) is not always linear (i.e., not represented by a matrix in coefficient space). That is the case for the wave equation (2.26), with a spatial operator of the form $\varphi \to e^{2\zeta}\Delta\varphi$. This equation is then decomposed as follows:

$$\frac{\partial^2\varphi}{\partial t^2} = (\lambda_2^{(t)} r^2 + \lambda_1^{(t)} r + \lambda_0^{(t)})\Delta\varphi + \sigma_\varphi ,$$

with

$$\sigma_\varphi = (e^{2\zeta} - \lambda_2^{(t)} r^2 + \lambda_1^{(t)} r + \lambda_0^{(t)})\Delta\varphi + e^{2\zeta}\frac{\partial\zeta}{\partial r}\frac{\partial\varphi}{\partial r} + \frac{\partial\zeta}{\partial t}\frac{\partial\varphi}{\partial t} + (\text{matter source terms})$$

and $\lambda_2^{(t)} r^2 + \lambda_1^{(t)} r + \lambda_0^{(t)}$ being an approximation of $e^{2\zeta(r,t)}$, allowing us to write the most important part of the spatial operator in a ''linear'' form. Finally, one writes $\partial^2\varphi/\partial t^2|_{t=t_J}$ with the second-order approximation and $\Delta\varphi_{t_J} = (\Delta\varphi_{t_{J+1}} + \Delta\varphi_{t_{J-1}})/2$ to make the integration scheme implicit. The boundary condition imposed on the outer edge of the grid (far away from the star) is that of an *outgoing wave*, meaning that the wave can be written as

$$\varphi(t,r) = \varphi_0 + \frac{1}{r}F\left(t - \frac{r}{c}\right), \tag{A3}$$

which is an exact condition for one-dimensional waves. Differentiating, one gets

$$\left.\frac{1}{c}\frac{\partial\varphi}{\partial t} + \frac{\partial\varphi}{\partial r} + \frac{(\varphi - \varphi_0)}{r}\right|_{\text{outer edge}} = 0. \tag{A4}$$

Actually, this is not the right boundary condition for a wave equation in curved space-time, however, since the boundary condition is imposed far away from the star (i.e., on a nearly flat space-time), a good approximation is obtained by taking as a boundary condition

$$\left. e^{-\zeta}\frac{\partial\varphi}{\partial t} + \frac{\partial\varphi}{\partial r} + \frac{\varphi}{r}\right|_{\text{outer edge}} = 0. \tag{A5}$$

3. Dynamical evolution

The integration procedure is quite similar to that of Gourgoulhon in [18]. All matter and field quantities are supposed to be known at some initial instant t_0, and one wants then to get them at $t_0 + \delta t$. First, one can compute the scalar field variables φ and Ξ at that time thanks to wave equation (2.26) and Eq. (2.27). Similarly, one gets the fluid quantities $\widetilde{E}$, U (and thus Γ), H, and $\widetilde{D}$, with their evolution equations (2.28), (2.29), (2.32), and (2.31). Then, one can deduce the metric coefficient $A(r, t_0 + \delta t)$ through Eqs. (2.23) and (2.11) [the integration constant is obtained by the condition $\forall t$, $A(r=0,t)=1$] and determine the fluid proper baryonic density $\widetilde{n}_B$, by inverting relation (2.16). The equation of state then gives the pressure $\widetilde{p}(\widetilde{n}_B)$.

Finally, one uses Eq. (2.25) to obtain $\nu(r, t_0 + \delta t)$, which is determined up to an additive constant. Since there is no Birkhoff theorem in scalar-tensor gravity, this constant cannot be determined by matching the interior solution to the exterior (static) one, used before. Even the exterior space-time is dynamic. Using a large grid (which is going far away from the star, typically $\sim 30 \times R_{\text{star}}$) enables the gravitational field to be in the weak-field regime at the outer edge of the grid allowing us to write with a good approximation

$$\forall t, A(R_{\text{out}}, t) \times N(R_{\text{out}}, t) = K_{AN}, \tag{A6}$$

K_{AN} being a constant determined for the static configuration ($K_{AN}=1$ for general relativity). One thus gets the integration constant for $\nu(r, t_0 + \delta t)$. Observing $A(R_{\text{out}})$ during the collapse, one sees that $\Delta A(R_{\text{out}}) \leqslant 10^{-5}$. This is quite lower than the overall committed error, see Appendix 4. Once $N(r,t)$ is obtained, the velocity V is deduced and all quantities are known at the instant $t_0 + \delta t$.

Time integration is performed by means of a second-order semi-implicit scheme (see previous sections), boundary conditions being imposed on the H, U system

$$\frac{1}{r^2}\frac{\partial}{\partial r}r^2 V|_{r=R_{\rm star}}=0 \tag{A7}$$

and on the wave equation (A5). Contrary to [18], the code is working with several domains. Each domain is partly comoving with the fluid, meaning that inside the star, both edges of a domain are comoving, the grid's velocity at each point being (linearly) interpolated. The edge of the outer domain is at rest [$V_{\rm grid}(r=R_{\rm out})=0$], and the grid's velocity between star's surface and this outer edge is interpolated at each point the same way. Typically, two domains have been used for the star's interior and three for the exterior, with about 65 points in each domain, which is considerably lower than the number of points used in finite difference schemes. A full run, with this multidomain spectral methods, took about 20 min of CPU time on an Onyx Silicon Graphics workstation (with a MIPS R4400, 200 MHz processor), for $\sim$20 000 time steps.

4. Tests

All equations have been checked using the MATHEMATICA algebraic code. More precisely, the Schwartz relation for Eqs. (2.23) and (2.24),

$$\frac{\partial^2 m}{\partial r\partial t}-\frac{\partial^2 m}{\partial t\partial r}=0,$$

was computed giving

$$\frac{\partial\varphi}{\partial t}\times[\Box_{g_*}\varphi+q_\pi\alpha(\varphi)T_*]$$
$$=\frac{\partial\widetilde{E}}{\partial t}+\frac{1}{r^2}\frac{\partial}{\partial r}[r^2(\widetilde{E}+\widetilde{p})V]$$
$$-[\text{right-hand side of Eq. (2.28)}]$$

which is consistent with Eqs. (2.26) and (2.28). Finally, setting $\varphi=0$ gives the equations of general relativity as described in [18].

For static configurations, the following test was performed. Considering the same equation of state as in [11] (EOS1 in this work), the same coupling function [$a(\varphi)=\exp(-3\varphi^2)$], and asymptotic scalar field value ($\varphi_0=0.0043$), we obtained the same dependence for the effective scalar coupling constant (the ratio between the scalar and the gravitational energies) on the star's baryonic mass (Fig. 2 of [11]). We also observed an increase of the maximal gravitational mass of neutron stars, when taking into account the scalar field, as it has been showed in Fig. 1 of [11].

The subroutine solving the wave equation has been checked by taking analytical solutions of simpler wave equations,

$$\frac{\partial^2\varphi}{\partial t^2}=W(t,r)^2\Delta\varphi, \tag{A8}$$

where $W(t,r)$ is a given function, and verifying that the discrepancy between numerical solution and the analytical one goes down as the square of the integration time step (second order scheme). For example,

$$\varphi(t,r)=\frac{\tanh(r)}{r}\ln(t+2)$$

which is the solution for $W(t,r)^2=\cosh(r)^2/2(2+t)^2\ln(t+2)$, was numerically obtained at 10^{-6} relative accuracy, with a time step which is $dt^J=1/100$ of the grid's radius, after 1000 iterations. The boundary condition was checked by looking for the remaining energy of the wave in the grid, after the wave was supposed to be gone. With the same time step as above, and for the usual wave equation ($\Box\varphi=0$), after 500 integrations, there remained 4.9×10^{-8} of the initial energy, this amount going down as $(dt^J)^4$, for the energy is the ''square'' of the amplitude. As it has been seen in the previous sections, a numerical grid partly comoving with the fluid was used. For this purpose, the wave equations have been adapted to such a grid and tested.

Finally, during dynamical evolution, a good test of overall accuracy was made by comparing the energy density $\widetilde{e}$ given by the baryonic density through the equation of state, to that deduced from $\widetilde{E}$ (which is an evolved quantity). The same is possible for H. On a whole run this error always stayed $<$few$\times10^{-3}$. The conservation of the baryonic number was verified with a relative accuracy better than 10^{-5}.

[1] T. Damour and G. Esposito-Farèse, Class. Quantum Grav. **9**, 2093 (1992).
[2] M. Fierz, Helv. Phys. Acta **29**, 128 (1956).
[3] P. Jordan, Z. Phys. **157**, 112 (1959).
[4] C. Brans and R.H. Dicke, Phys. Rev. **124**, 925 (1961).
[5] P.G. Bergmann, Int. J. Theor. Phys. **1**, 25 (1968).
[6] K. Nordtvedt, Astrophys. J. **161**, 1059 (1970).
[7] R.V. Wagoner, Phys. Rev. D **1**, 3209 (1970).
[8] C.G. Callan, D. Friedman, E.J. Martinec, and M.J. Perry, Nucl. Phys. **B262**, 593 (1985).
[9] T. Damour and A.M. Polyakov, Nucl. Phys. **B423**, 532 (1994).
[10] P.J. Steinhardt and F.S. Accetta, Phys. Rev. Lett. **64**, 2740 (1990).
[11] T. Damour and G. Esposito-Farèse, Phys. Rev. Lett. **70**, 2220 (1993).
[12] T. Damour and G. Esposito-Farèse, Phys. Rev. D **54**, 1474 (1996).
[13] A. Giazotto, Phys. Rep. **182**, 365 (1989).
[14] A. Abramovici *et al.*, Science **256**, 325 (1992).
[15] M. Shibata, K. Nakao, and T. Nakamura, Phys. Rev. D **50**, 6058 (1994).
[16] M.A. Scheel, S.L. Shapiro, and S.A. Teukolsky, Phys. Rev. D **51**, 4236 (1995).
[17] T. Harada, T. Chiba, K. Nakao, and T. Nakamura, Phys. Rev. D **55**, 2024 (1997).
[18] E. Gourgoulhon, Astron. Astrophys. **252**, 651 (1991).

[19] R. Arnowitt, S. Deser, and C.W. Misner, in *Gravitation*, edited by L. Witten (Wiley, New York, 1962).
[20] T. Piran, in *Rayonnement gravitationnel – Les Houches 1982*, edited by N. Deruelle and T. Piran (North-Holland, Amsterdam, 1983).
[21] J. Diaz-Alonso and J.M. Ibañez-Cabanell, Astrophys. J. **291**, 308 (1985).
[22] M. Salgado, S. Bonazzola, E. Gourgoulhon, and P. Haensel, Astron. Astrophys. **291**, 155 (1994).
[23] R. Coquereaux and G. Esposito-Farèse, Ann. Inst. Henri Poincaré **52**, 113 (1990).
[24] S. Bonazzola and J.A. Marck, Astron. Astrophys. **164**, 300 (1986).
[25] R.V. Wagoner and D. Kalligas, in *Relativistic Gravitation and Gravitational Radiation*, edited by J. A. Marck and J. P. Lasota (Cambridge University Press, Cambridge, England, 1997).
[26] T. Harada, Prog. Theor. Phys. **98**, 359 (1997).
[27] B. Caron *et al.*, in *Gravitational Waves: Sources and Detectors*, edited by I. Ciufolini and F. Fidecaro (World Scientific, Singapore, 1997).
[28] S. Bonazzola and J.A. Marck, Astron. Astrophys. **267**, 623 (1993).
[29] T. Zwerger and E. Müller, Astron. Astrophys. **320**, 209 (1997).
[30] S. Bonazzola and J.A. Marck, J. Comput. Phys. **87**, 201 (1990).
[31] S. Bonazzola, E. Gourgoulhon, and J.A. Marck, in *Relativistic Gravitation and Gravitational Radiation*, edited by J. A. Marck and J. P. Lasota (Cambridge University Press, Cambridge, England, 1997).